JCI The Journal of Clinical Investigation

Immunoglobulin light chains generate proinflammatory and profibrotic kidney injury

Wei-Zhong Ying, … , Lisa M. Curtis, Paul W. Sanders

J Clin Invest. 2019;129(7):2792-2806. https://doi.org/10.1172/JCI125517.

Research Article **Hematology** **Nephrology**

Because of the less-than-robust response to therapy and impact on choice of optimal chemotherapy and prognosis, chronic kidney disease has drawn attention in the treatment of multiple myeloma, a malignant hematologic disorder that can produce significant amounts of monoclonal immunoglobulin free light chains (FLCs). These low-molecular-weight proteins are relatively freely filtered through the glomerulus and are reabsorbed by the proximal tubule. The present study demonstrated that during the process of metabolism of immunoglobulin FLCs, ROS activated the STAT1 pathway in proximal tubule epithelium. STAT1 activation served as the seminal signaling molecule that produced the proinflammatory molecule IL-1β, as well as the profibrotic agent TGF-β by this portion of the nephron. These effects occurred in vivo and were produced specifically by the generation of hydrogen peroxide by the V_L domain of the light chain. To the extent that the experiments reflect the human condition, these studies offer insights into the pathogenesis of progressive kidney failure in the setting of lymphoproliferative disorders, such as multiple myeloma, that feature increased circulating levels of monoclonal immunoglobulin fragments that require metabolism by the kidney.

Immunoglobulin light chains generate proinflammatory and profibrotic kidney injury

Wei-Zhong Ying,[1] Xingsheng Li,[1] Sunil Rangarajan,[1] Wenguang Feng,[1] Lisa M. Curtis,[1,2,3] and Paul W. Sanders[1,2,3]

[1]Department of Medicine and [2]Department of Cell, Developmental, and Integrative Biology, University of Alabama at Birmingham, Birmingham, Alabama, USA. [3]Department of Veterans Affairs Medical Center, Birmingham, Alabama, USA.

Because of the less-than-robust response to therapy and impact on choice of optimal chemotherapy and prognosis, chronic kidney disease has drawn attention in the treatment of multiple myeloma, a malignant hematologic disorder that can produce significant amounts of monoclonal immunoglobulin free light chains (FLCs). These low-molecular-weight proteins are relatively freely filtered through the glomerulus and are reabsorbed by the proximal tubule. The present study demonstrated that during the process of metabolism of immunoglobulin FLCs, ROS activated the STAT1 pathway in proximal tubule epithelium. STAT1 activation served as the seminal signaling molecule that produced the proinflammatory molecule IL-1β, as well as the profibrotic agent TGF-β by this portion of the nephron. These effects occurred in vivo and were produced specifically by the generation of hydrogen peroxide by the V_L domain of the light chain. To the extent that the experiments reflect the human condition, these studies offer insights into the pathogenesis of progressive kidney failure in the setting of lymphoproliferative disorders, such as multiple myeloma, that feature increased circulating levels of monoclonal immunoglobulin fragments that require metabolism by the kidney.

Introduction

Multiple myeloma, a malignant plasma cell disorder, has an incidence rate of approximately 1.1% among all malignancies and constitutes 12%–13% of hematologic malignancies in the United States (1). Nearly half of the patients who have myeloma have concomitant kidney injury (defined as serum creatinine ≥1.3 mg/dl) (2); approximately 19% have an estimated glomerular filtration rate below 30 ml/min/1.73 m^2 at the time of diagnosis (3); and 8% of patients require renal replacement therapy (4). Myeloma is considered the most common malignancy that leads to end-stage kidney disease (5). An increase in the serum creatinine concentration beyond 2.0 mg/dl portends a poor prognosis, with an approximate 42% reduction in median survival compared with patients who did not have renal dysfunction (2). One large study concluded that the reversibility of renal function was a more important prognostic factor than plasma cell response to chemotherapy (6). Thus, the level of renal function is a critical determinant of prognosis in multiple myeloma (4, 6).

Most patients with myeloma and clinical manifestations of kidney failure have tubulointerstitial disease due to cast nephropathy (7, 8). Immunoglobulin free light chains (FLCs) are responsible for this type of kidney injury, and a prompt reduction in serum FLCs is critical for renal function recovery (6, 9, 10). However, even with modern chemotherapeutic options and extracorporeal therapies designed to target the removal of monoclonal FLCs, reductions in circulating FLCs require time (10–16), permitting the progression of kidney disease, which may occur rapidly with persistently elevated serum FLC levels (17). New insights into the pathogenesis and management of this progressive kidney disease are therefore critical.

In the process of catabolism by the kidney, certain monoclonal FLCs can promote significant changes in epithelial cell biology. Several studies have now shown that monoclonal FLCs are biologically active proteins that can generate hydrogen peroxide in amounts sufficient to activate intracellular redox-sensitive signaling pathways (18–24). The present study tested the hypothesis that critical redox-sensitive pathways are activated during the metabolism of monoclonal FLCs in the proximal tubule, the site of uptake and catabolism of circulating FLCs (25), and promote kidney injury. The following experiments identified an intracellular signal transduction mechanism that generated a proinflammatory and profibrotic milieu in the kidney and featured STAT1.

▶ Related Commentary: p. 2660

Authorship note: WZY and XL contributed equally to this work.
Conflict of interest: The authors have declared that no conflict of interest exists.

Submitted: October 11, 2018; **Accepted:** April 9, 2019; **Published:** June 17, 2019.
Reference information: *J Clin Invest*. 2019;129(7):2792–2806.
https://doi.org/10.1172/JCI125517.

Results

Monoclonal κ and λ family FLCs activate the redox-sensitive JAK2/STAT1 pathway in human kidney epithelial cells. Initial experiments determined that incubation of human kidney epithelial cells with 2 different FLCs, termed κ2 and λ3, promoted the activation of JAK2 and STAT1. AG-490, a specific JAK2/3 tyrosine kinase blocker (26), inhibited the activation of this pathway (Figure 1, A and B). Immunofluorescence confocal microscopy also showed that incubation of the cells with the κ2 and λ3 FLCs promoted the activation of STAT1 and nuclear translocation of phosphorylated STAT1 (p-STAT1) (Figure 1C). Overnight incubation of human kidney 2 (HK-2) cells with 6 different human FLCs (three κ and three λ) produced this same effect on STAT1 activation (data not shown).

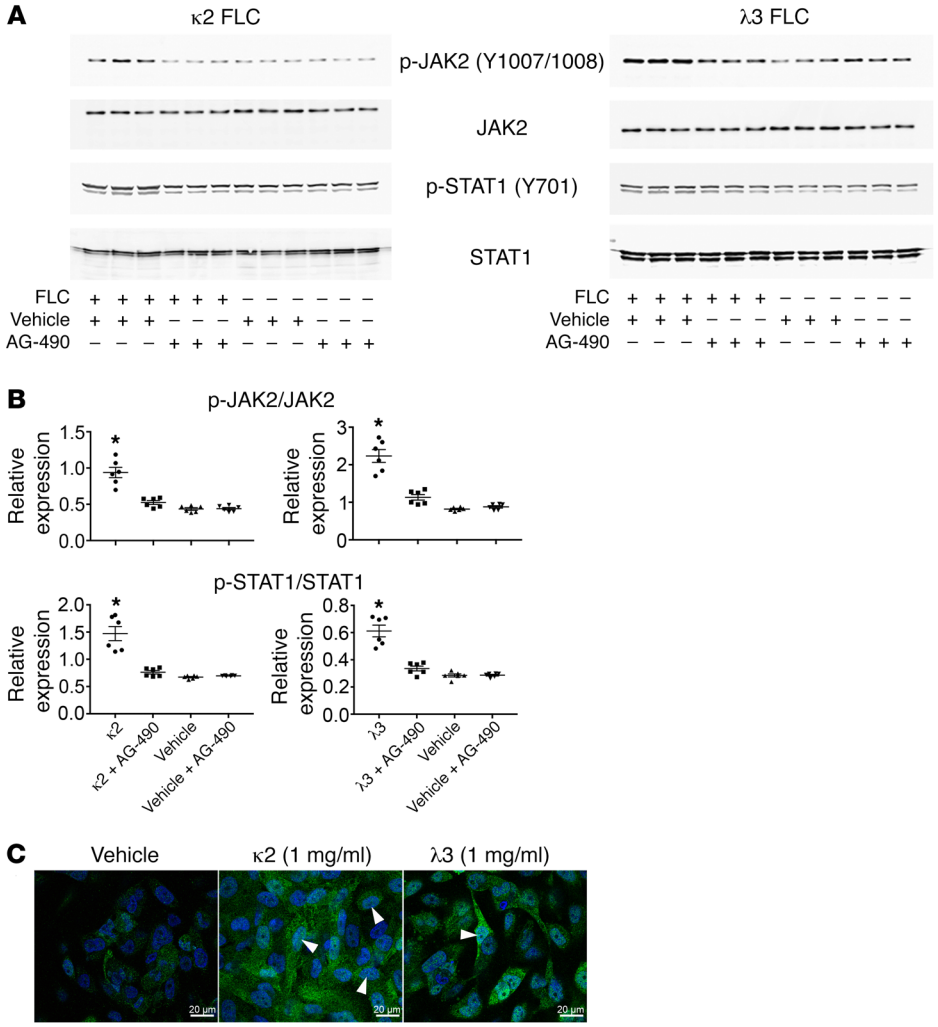

Figure 1. Monoclonal FLCs activate the JAK2/STAT1 pathway. (**A** and **B**) Western blot analysis showed activation of both JAK2 and STAT1 in HK-2 cells incubated with 2 different monoclonal FLCs (1 mg/ml). The JAK2/3 inhibitor AG-490 (30 μM) inhibited these responses (n = 6 experiments in each group). Data are expressed as the mean ± SEM. *$P < 0.0001$ compared with the other 3 groups (ANOVA). (**C**) Confocal microscopic images supported the Western blot analyses by showing that overnight incubation of HK-2 cells with the 2 different FLCs increased p-STAT1 (Y701) (green fluorescence) in the cytoplasm and nuclei (arrowheads). Nuclei were counterstained blue. This representative experiment was repeated once. Scale bars: 20 μm.

Incubation of human kidney epithelial cells with monoclonal FLC–activated caspase-1 and increased production of IL-1β and active TGF-β. Overnight incubation of HK-2 cells with each of 6 unique monoclonal FLCs activated intracellular caspase-1 and increased IL-1β and active TGF-β in the medium. The addition of AG-490 inhibited these effects (Figure 2, A–C). These experiments were then repeated using both AG-490 (30 μM) and ruxolitinib (1 μM), a clinically available JAK inhibitor (27, 28). In a similar fashion, both inhibitors prevented FLC-mediated activation and production of caspase-1 (Figure 2D), IL-1β (Figure 2E), and active TGF-β (Figure 2F). To confirm causality, HK-2 cells were pretreated with either STAT1 siRNA or a nontargeting siRNA and then treated with the κ2 and λ3 FLCs. Cells treated with STAT1 siRNA showed significantly reduced intracellular caspase-1 activity, IL-1β release into the medium, and total and active TGF-β in the medium (Supplemental Table 1; supplemental material available online with this article; https://doi.org/10.1172/JCI125517DS1), as well as p-STAT1 (Y701) and p-SMAD2 levels in the cell lysates in response to the FLCs (Figure 3). These findings indicate that the STAT1 pathway is critically involved in the generation of both IL-1β and TGF-β by proximal tubular epithelium.

The V_L domain of FLCs activates proinflammatory and profibrotic pathways through redox signaling. The capability of FLCs to alter proximal tubular cell function greatly exceeded the activating effect of other proteins, such as albumin (29, 30). Recent evidence showed that monoclonal FLCs are biologically active proteins that can generate redox signaling, particularly in proximal tubule cells following endocytosis (18–24). Because prior studies demonstrated that the hydrogen peroxide scavenger 1,3-dimethyl-2-thiourea (DMTU) inhibited the effects of FLCs on redox signaling (18, 21), DMTU (30 mM) was concomitantly added to the medium with the FLCs. Overnight incubation with DMTU inhibited STAT1 activation by both the κ and λ FLCs (Figure 4, A and B).

We explored the mechanism by which redox-signaling events were generated. Using the SWISS-MODEL Workspace (31–34), we generated a molecular model of the V_L domain of a κ FLC (Figure 5). The sequence shared 95.58% homology with a previously crystalized light chain in the repository. The model showed a unique molecular structure of the core of the V_L domain, with the indole ring of the invariant tryptophan extending into the pocket. As a proof of concept of the role of the tryptophan in generating H_2O_2 and redox signaling, we synthesized 2 recombinant proteins and used them in a series of experiments. Both proteins shared sequence homology with the V_L domain of a κII subfamily FLC, but one of the proteins contained a W40G substitution; these proteins were termed V_L and mutant V_L (Figure 5). When compared

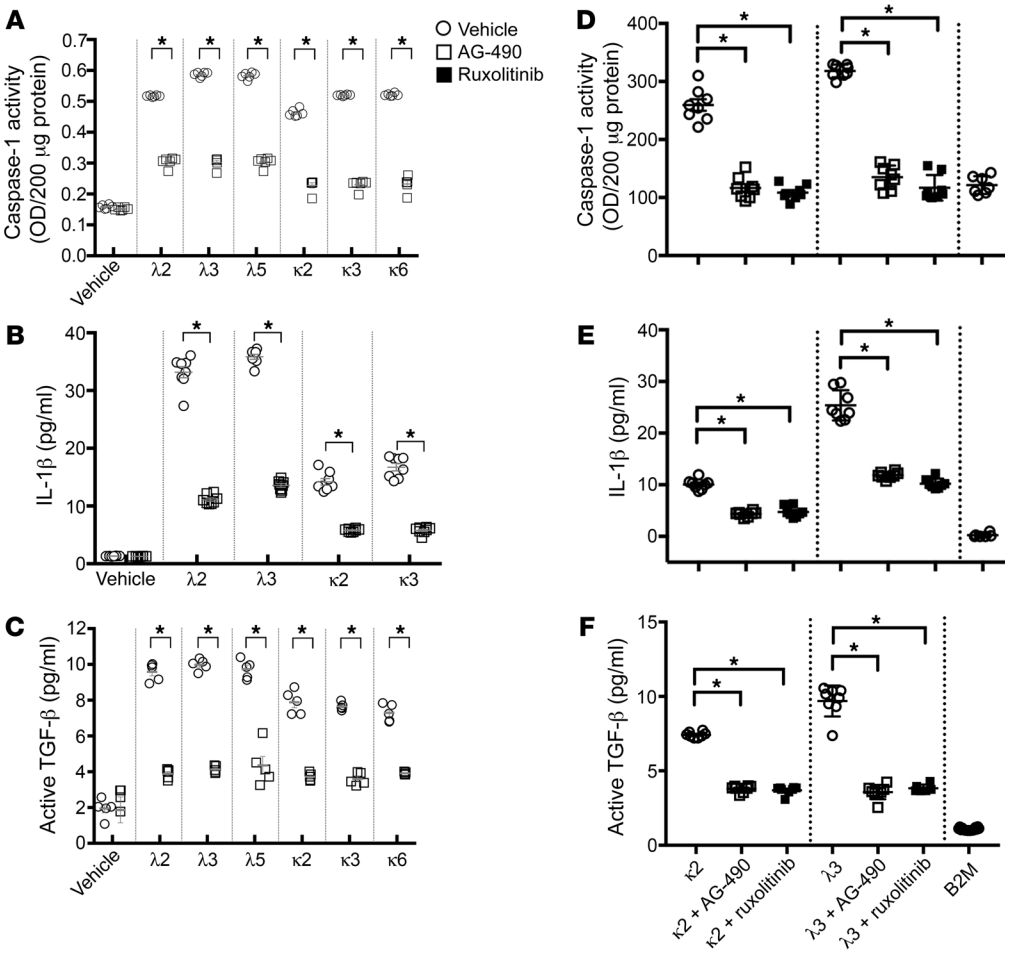

Figure 2. Six unique monoclonal FLCs activate the JAK/STAT pathway and increase caspase-1 activity in HK-2 cells and increase IL-1β and active TGF-β in the medium. (**A**) Results of the colorimetric assay of caspase-1 activity (n = 6 in each group). The main effects of the FLCs and the interaction effect between the FLCs and AG-490 on caspase-1 activity were significant at a P value of less than 0.0001. *P < 0.0001 compared with the corresponding group. (**B**) Results of the ELISA for IL-1β (n = 6 in each group). The main effects of the FLC and the interaction effect between the FLC and AG-490 on IL-1β showed that all effects were significant at a P value of less than 0.0001. *P < 0.0001 compared with the corresponding group. (**C**) Results of the TGF-β assay (n = 5 in each group). *P <0.0001 compared with the corresponding group. (**D**–**F**) Comparison of the effects of the addition of the JAK inhibitor ruxolitinib and AG-490 on caspase-1 activity (determined using a fluorometric assay), IL-1β, and active TGF-β (n = 6–8 samples in each group). Ruxolitinib produced results that did not differ from those seen with AG-490. *P < 0.0001 compared with the corresponding group. Also, compared with human B2M, another low-molecular-weight protein control, incubation of HK-2 cells with the 2 different FLCs (κ2 and λ3) produced greater (P < 0.0001) increases in caspase-1 activity, IL-1β concentration, and active TGF-β. Data are expressed as the mean ± SEM and were analyzed using factorial ANOVA for the data in **A**–**C** and by ANOVA for the data in **D**–**F**.

with another recombinant protein that had an identical sequence except for a W40G substitution (mutant V_L), the mutant V_L produced much less hydrogen peroxide in vitro under the proper conditions (18) (Figure 6). When compared with the recombinant V_L with the W40G substitution and 2 other control proteins, chicken egg albumin (CEA) and human β-2 microglobulin (B2M), overnight incubation of HK-2 cells with the recombinant V_L protein increased the intracellular activation of STAT1 and caspase-1 and promoted the production of IL-1β and active TGF-β. These findings recapitulated the data obtained using intact monoclonal FLCs.

The mechanism of activation of TGF-β involves the expression of αvβ6 integrin by proximal tubule epithelial cells. We performed flow cytometric studies using an anti–integrin subunit β 6 (ITGB6) antibody with HK-2 cells after overnight incubation with the κ2 and λ3 FLCs to detect the surface expression of the β6 subunit of αvβ6 integrin. Untreated epithelial cells and epithelial cells previously transfected with plasmids containing either ITGB6 shRNA or nontargeting shRNA were incubated overnight in medium containing the κ2 and λ3 FLCs. For untreated cells and HK-2 cells pretreated with the nontargeting shRNA, we found that both FLCs increased the numbers of cells expressing ITGB6 on the cell surface and that cells pretreated with ITGB6 shRNA did not increase the cell-surface expression of ITGB6 in response to incubation with the FLCs. Pretreatment with ITGB6 shRNA prevented the activation of TGF-β (Figure 7).

Stat1-deficient mice are protected from FLC-mediated activation of proinflammatory and profibrotic pathways. Colonies of *Stat1*$^{+/+}$ and *Stat1*$^{-/-}$ mice were generated, and their genotypes were confirmed (Supplemental Figures 1 and 2). Mice of both strains were injected daily for 10 days with vehicle or a lower dose (κ2-d1) (0.033 mg/g BW) or higher dose (κ2-d2) (0.165 mg/g BW) of the monoclonal κ2 FLC, which had been used in earlier in vivo experiments in rats to produce cast nephropathy, but at a much larger dose (35). In the present study, on day 10, the mean serum creatinine levels did not differ among the groups studied (Figure 8A). When the κ2-d2 treatment period was extended to 30 days, the mean serum creatinine concentration increased specifically in the κ2-d2–treated group of *Stat1*$^{+/+}$ mice (Figure 8B). Subsequent studies were therefore limited to 10 days to reduce confounding factors from the development of clinically identified chronic kidney disease. Immunofluorescence microscopy showed colocalization of the κ FLC with *Lotus tetragonolobus* lectin (LTL), a carbohydrate-binding protein that binds to the brush border and identifies differentiated proximal tubules (36), in both *Stat1*$^{-/-}$ and *Stat1*$^{+/+}$ mice (Supplemental Figure 3). The higher dose of κ2-d2 produced mild tubular injury in the *Stat1*$^{+/+}$ mice, as demonstrated by increased urinary excretion of albumin (37) and kidney injury

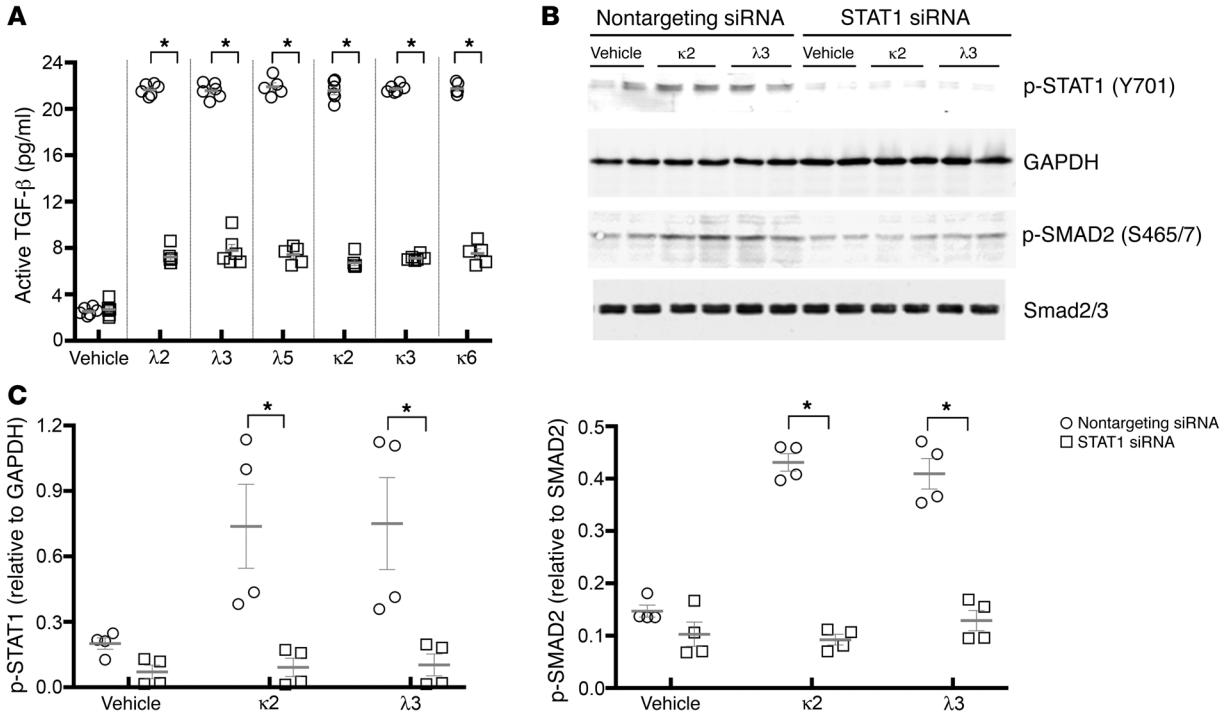

Figure 3. Knockdown of STAT1 inhibits FLC-mediated increases in TGF-β in medium and p-STAT1 and p-SMAD2 levels in HK-2 cells. (**A**) All tested FLCs increased active TGF-β by HK-2 cells treated with a nontargeting siRNA, but not by HK-2 cells pretreated with an siRNA that targeted STAT1 (n = 5–6 in each group). Data are expressed as the mean ± SEM. Factorial ANOVA comparing the main effects of the FLC and the interaction effect between the FLC and siRNA on TGF-β showed that all effects were significant at a P value of less than 0.0001. The main effect for the siRNA yielded an F ratio of F(1, 66) = 6203, $P < 0.0001$. The interaction effect was significant: F(6, 66) = 185.8, $P < 0.001$. *$P < 0.0001$ compared with the corresponding group. (**B**) Western blot and (**C**) densitometric analyses showed the effect of siRNA treatment on p-STAT1 and p-SMAD2 (n = 4 in each group). Data are expressed as the mean ± SEM. Factorial ANOVA comparing the main effects of the FLC and the interaction effect between the FLC and siRNA on p-STAT1 showed that the main effect for the FLC yielded an F ratio of F(2, 18) = 3.724, $P = 0.044$, and that the effect of the siRNA yielded an F ratio of F(1, 18) = 0.0001. The interaction effect was not significant. *$P = 0.014$ compared with the corresponding group. For p-SMAD2, factorial ANOVA comparing the main effects of the FLC and the interaction effect between the FLC and the siRNA showed that all effects were significant at a P value of less than 0.0001. The main effect for the siRNA yielded an F ratio of F(1, 18) = 194.3, $P < 0.0001$. The interaction effect was significant at F(2, 18) = 32.19, $P < 0.0001$. *$P < 0.0001$ compared with the corresponding group.

molecule 1 (KIM-1), an inducible, apically expressed molecule that reflects tubular epithelial cell injury (38, 39), but the *Stat1*$^{-/-}$ mice were protected from this injury (Figure 8, C and D). Colocalization of κ FLC with KIM-1 was observed only in the *Stat1*$^{+/+}$ group (Figure 8, E and F). Blinded analyses of the tissue sections also showed that only kidneys from the *Stat1*$^{+/+}$ mice had tubular epithelial disruption (Figure 8G). We did not observe cast nephropathy in either mouse strain using these 2 FLC doses. The apoptosis we observed in both strains at the higher FLC dose may reflect activation of other redox-sensitive pathways independent of STAT1 (19).

Stat1 mRNA was not present in the kidney cortex of *Stat1*$^{-/-}$ mice (Figure 9A). STAT1 protein was also absent from the kidney cortex of *Stat1*$^{-/-}$ mice, but the κ2 FLCs promoted an increase in the activation of STAT1 in WT mice (Supplemental Figure 4). We found that steady-state levels of mRNA and activity of caspase-1 were increased only in the kidney cortex of *Stat1*$^{+/+}$ mice treated with the κ2 FLCs (Figure 9, B and D). Both IL-1β (Figure 9, C and E) and TGF-β (Figure 9F) were increased in a dose-dependent fashion in the kidney cortex of FLC-treated *Stat1*$^{+/+}$ mice, but not in *Stat1*$^{-/-}$ mice. Immunofluorescence microscopy confirmed that the proximal tubule was the source of IL-1β (Figure 10). Associated with the increase in IL-1β was an increase in ITGB6 expression and accumulation of neutrophils (Figure 11A) in the kidney cortex of the κ2-d2–treated group of *Stat1*$^{+/+}$ mice, but not in the *Stat1*$^{-/-}$ mice. This sterile inflammatory response included specialized macrophages that expressed heme oxygenase-1 (HO-1), indicating an M2 phenotype that has been shown to be involved not only in limiting inflammation but also in promoting fibrogenesis (Figure 11B) (40, 41). Consistent with the immunofluorescence studies showing expression of ITGB6 in the proximal tubule (Figure 11A), both ITGB6 and p-SMAD2/3 levels increased in cortical lysates from the FLC-treated *Stat1*$^{+/+}$ mice, but not in those from *Stat1*$^{-/-}$ mice (Figure 12). ITGB6 and p-SMAD2/3 levels in the kidney cortical lysates were directly correlated (Supplemental Figure 5). Picrosirius red staining imaged under polarized light revealed an increase in interstitial deposition of collagen only in the *Stat1*$^{+/+}$ mouse kidney (Figure 13). These findings were identified in the setting of mild morphological evidence of tubular epithelial cell injury (Figure 8G).

Discussion

One function of the proximal tubule is to conserve amino acids by reclaiming proteins that are filtered through the glomerulus. FLCs are low-molecular-weight proteins that are relatively freely

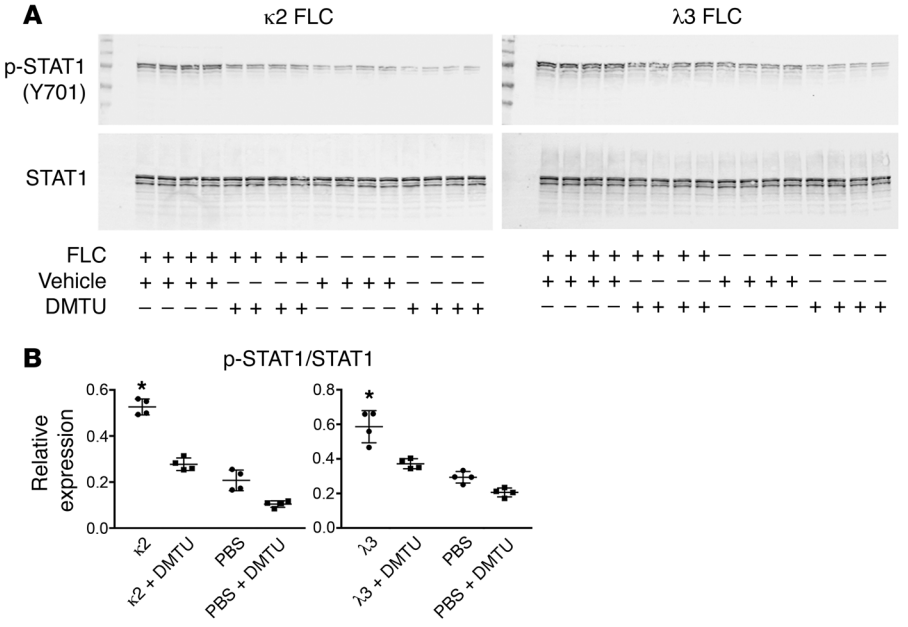

Figure 4. DMTU inhibited the FLC-mediated activation of STAT1 in HK-2 cells. (**A** and **B**) Results of coincubation of HK-2 cells with DMTU and either the κ or the λ FLC (n = 4 samples in each group). Data are expressed as the mean ± SEM. Factorial ANOVA comparing the main effects of the FLC and the interaction effect between the FLC and DMTU on p-STAT1 and STAT1 showed that all effects were significant at a P value of less than 0.05. The main effect for DMTU yielded an F ratio of F(1, 12) = 119.9, $P < 0.0001$ for the κ FLC, and an F ratio of F(1, 12) = 32.25, $P < 0.0001$ for the λ FLC. The interaction effect was significant for both the κ and λ FLCs: F(1, 12) = 20.64, $P = 0.0007$ and F(1, 12) = 5.676, $P = 0.0346$, respectively. The effect of both the κ and λ FLCs on STAT1 activation was greater than that for the other 3 groups (*$P < 0.0001$).

filtered during the production of a glomerular ultrafiltrate and are reabsorbed by the proximal tubule, where they undergo hydrolysis (25). The capability of FLCs to alter proximal tubular cell function greatly exceeded the biological effects of other proteins, such as albumin (29, 30). The present studies uncovered a series of unique pathophysiological processes in the kidney and demonstrated for the first time to our knowledge that: (a) FLCs activated STAT1 in proximal tubule epithelium in vitro and in vivo; (b) the V_L domain of the FLC was sufficient to induce the redox signaling events; (c) FLCs activated caspase-1 and promoted the production of IL-1β by the proximal tubule, producing an inflammatory reaction in the interstitium in vivo; and (d) FLCs activated TGF-β and SMAD2/3 signaling through integrin αvβ6 and promoted collagen deposition in the interstitium of *Stat1*$^{+/+}$ mice. Absorption of monoclonal FLCs into the proximal tubule therefore resulted in a proinflammatory/fibrotic state that developed early in the course of the disease and featured STAT1 as the core signaling molecule that produced IL-1β, a potent inflammatory molecule (42), as well as TGF-β, by this portion of the nephron (Figure 14). Because TGF-β is a critical profibrotic agent that promotes the generation of myofibroblasts in the kidney (43) and IL-1β has recently been shown to activate a metabolic switch in stromal cells to drive matrix protein formation (44), we propose that these agents work in concert to promote kidney fibrosis.

Prior studies established that some but not all FLCs produce hydrogen peroxide in sufficient quantities to activate intracellular signaling mechanisms (18–22). On the basis of studies from the Wentworth laboratory that uncovered the capability of IgG to catalyze the oxidation of water to produce hydrogen peroxide (45–49), the present studies tested whether hydrogen peroxide is produced specifically by a mechanism intrinsic to the physicochemical features of the V_L domain. In particular, studies using xenon gas identified in the V_L domain, a cavity within the hydrophobic core generated by the highly conserved β sheets and containing an invariant tryptophan (47) (Figure 5). A recombinant protein that shares sequence homology with the V_L domain of a κII subfamily FLC produced hydrogen peroxide and replicated the findings obtained using intact human monoclonal FLCs. Our studies also demonstrated a critical role in this process for the conserved tryptophan at amino acid residue 40, since another recombinant protein that had an identical sequence except for a W40G substitution generated much less hydrogen peroxide in vitro under the appropriate conditions (18). Finally, the demonstration of activation of this pathway by hydrogen peroxide was consistent with reports that showed STAT1 activation by hydrogen peroxide in other cell types that included vascular smooth muscle cells (50) and fibroblasts (51).

Monoclonal FLCs therefore join a growing list of endogenous sterile activators of the cascade that generates IL-1β (52). FLCs activated caspase-1 (Figure 2A and Figure 9D), which has been shown to cleave and activate this potent mediator of inflammation (53). A peritubular inflammatory reaction accompanied the activation of IL-1β (Figure 10). There are multiple potential pathways that activate TGF-β, but because the STAT1 siRNA experiments also showed direct involvement in the production of TGF-β (Figure 3), we considered the role of a STAT1-dependent, αvβ6-dependent activation of TGF-β, as demonstrated in other disease conditions (54–57). Epithelial cells express the integrin αvβ6, which binds to the RGD sequence on the latency-associated peptide (LAP) that binds TGF-β, releasing the active form of the molecule to promote the pathological activity of TGF-β (58). Flow cytometric experiments using HK-2 cells incubated with monoclonal FLCs showed increased expression of the β6 subunit of αvβ6 (ITGB6) on the cell surface, which correlated with increased production of TGF-β, whereas decreased surface expression using ITGB6 shRNA reduced FLC-mediated production of active TGF-β (Figure 7). FLCs promoted an increase in the expression of ITGB6 and p-SMAD2/3 in kidney cortex in vivo (Figure 11 and Figure 12), a dose-dependent increase in TGF-β in renal cortical lysates (Figure 9), and collagen deposition in the interstitium (Figure 13). Because we also did not observe these effects in *Stat1*$^{-/-}$ mice, the findings uncovered an FLC-induced, STAT1-depen-

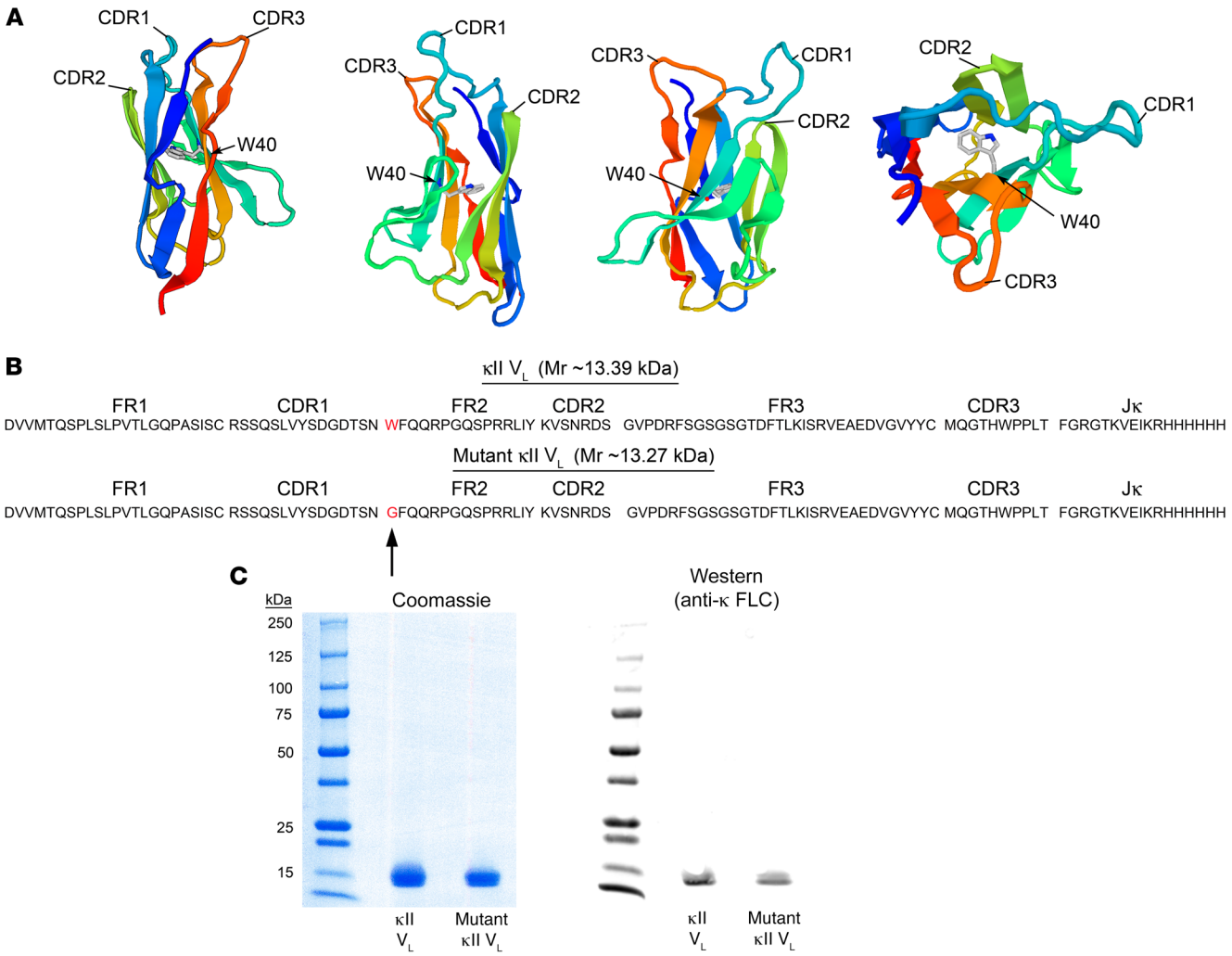

Figure 5. Production of a recombinant V_L protein and a W40G mutant of the V_L domain. (**A**) SWISS-MODEL Workspace (31, 32) and SWISS-MODEL Repository (33, 34) were used to generate a model of the V_L domain of a κII subfamily FLC. The framework (FR1, FR2, FR3 in **B**) regions are β sheets that developed a core pocket. Seen within the core was the indole ring portion (gray) of an invariant tryptophan at residue 40. (**B**) The sequences of the V_L and mutant V_L were identical, except for the substitution of glycine for tryptophan at amino acid residue 40. (**C**) Coomassie-stained gel showed the expected sizes of the 2 recombinant proteins, and Western blot analysis using an anti–human κ FLC confirmed antibody recognition of both recombinant proteins.

dent, αvβ6-dependent activation of TGF-β by the proximal tubule that led to interstitial fibrosis (Figure 14).

FLC-mediated tubulointerstitial kidney disease is complicated by proximal tubule damage, which may also indirectly activate inflammatory and fibrotic pathways (59). This potential complication of our in vivo studies was mitigated in part by the responses we observed on day 10, when serum creatinine levels had not yet increased. Data from the cell culture system provided a mechanistic understanding of the process in the absence of tubular atrophy and loss. Therefore, tubular damage and activation of proinflammatory and fibrotic pathways in the proximal tubule may work in concert in the progression of FLC-mediated chronic kidney disease. Because both processes are driven by FLCs, therapy that targets reductions in circulating FLCs is critical. In this regard, early studies have shown a therapeutic benefit of bortezomib in reducing circulating immunoglobulins and immunoglobulin fragments. However, these modern chemotherapeutic options that also include extracorporeal therapies designed to target the removal of monoclonal FLCs require time to reduce circulating FLCs (10–16). To the extent that these experiments reflect the human condition, the present study offers insights into the pathophysiology of FLC-mediated chronic kidney disease and is the first to our knowledge to recognize that ruxolitinib, which also inhibits the JAK/STAT pathway in myeloma cells and demonstrates antiproliferative activity (28), may have therapeutic potential in multiple myeloma–related tubulointerstitial disease.

Methods

Cells and reagents

Human proximal tubular epithelial cells. HK-2 cells, which have been well characterized (60), were obtained from the American Type Culture Collection (ATCC). Monolayers of HK-2 cells were grown on 6-well plates (Corning-Costar, Corning Life Sciences) that were precoated with 5 μg/cm² type 1 collagen (Rat Tail Collagen Type 1, Invit-

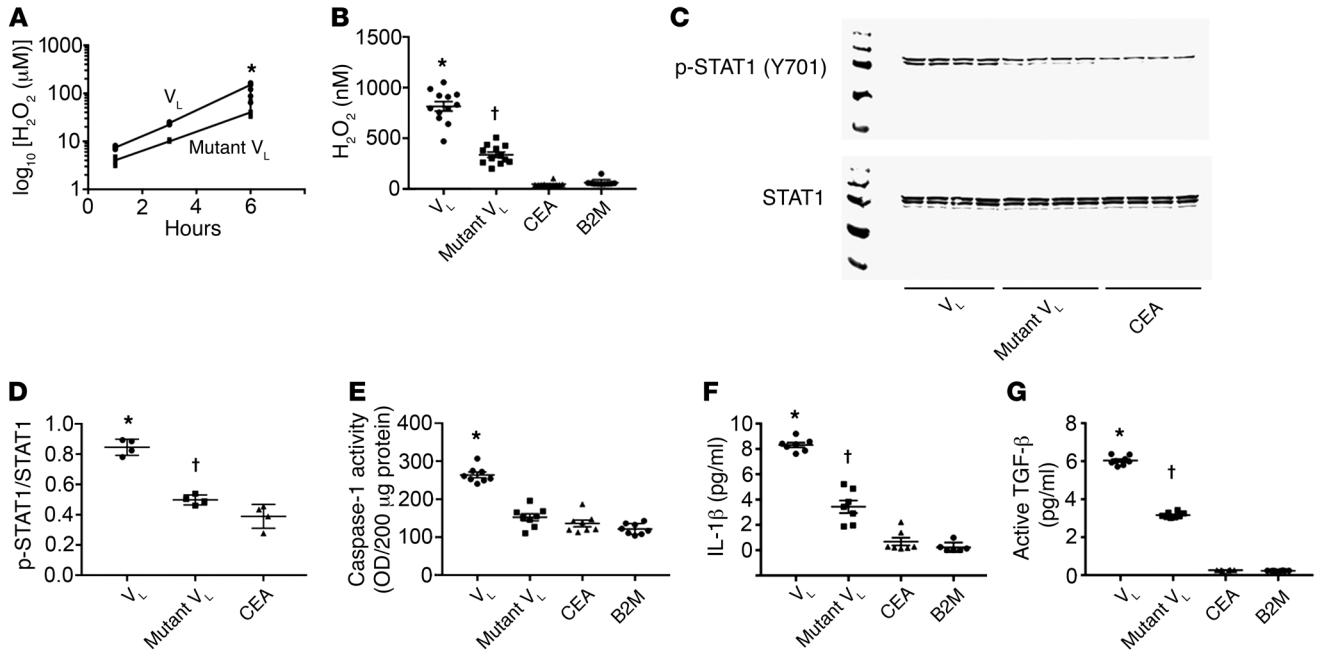

Figure 6. The recombinant V_L domain of a κII subfamily FLC, but not the mutant V_L, activates the proximal tubule to produce IL-1β and TGF-β. The recombinant V_L produced more hydrogen peroxide in vitro with exposure to (**A**) UV radiation (n = 10–11 at each time point) and (**B**) human proximal tubular epithelial cells (n = 5–6 experiments in each group). (**C** and **D**) The recombinant V_L also activated STAT1 (n = 4 experiments in each group); (**E**) increased caspase-1 activity (n = 7–8 experiments in each group); (**F**) increased IL-1β release (n = 4–7 experiments in each group); and (**G**) increased active TGF-β (n = 6–12 experiments in each group). Data are expressed as the mean ± SEM. *P < 0.0001 compared with other groups; †P < 0.05 versus controls (CEA and B2M, if shown) (ANOVA).

rogen, Thermo Fisher Scientific) and incubated at 37°C with 5% CO_2 and 95% air in keratinocyte serum-free medium (K-SFM) (Gibco, Invitrogen, Thermo Fisher Scientific) supplemented with recombinant human epidermal growth factor (5 ng/ml) and bovine pituitary extract (50 μg/ml). Medium was exchanged at 48-hour intervals, and the cells were not use beyond 25 to 30 passages.

Human immunoglobulin FLCs. Six unique human monoclonal FLCs (three and three) were purified using standard methods from the urine of patients with multiple myeloma, light chain proteinuria, and clinical evidence of significant renal damage that was presumed to be cast nephropathy. These proteins were arbitrarily labeled κ2, κ3, κ6, λ2, λ3, and λ5. The FLCs were determined to be endotoxin free.

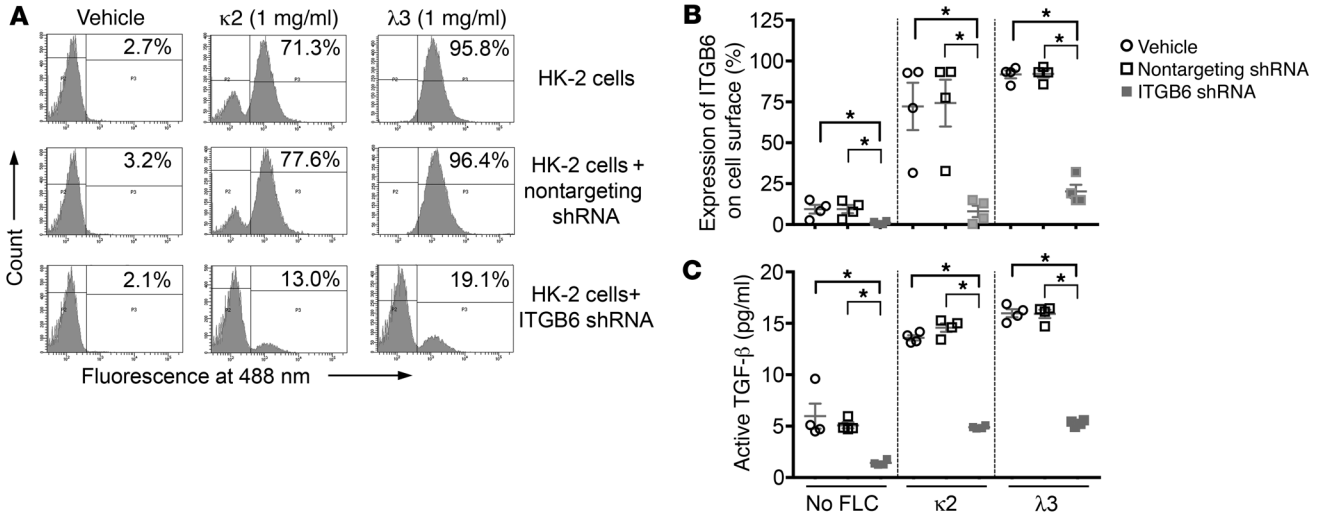

Figure 7. Overnight incubation of HK-2 cells with 2 different monoclonal FLCs promotes the expression of ITGB6 on the cell surface. (**A** and **B**) Flow cytometric studies demonstrated that both the κ2 and λ3 FLCs increased the number of cells expressing ITGB6 (n = 4 experiments in each group). Pretreatment of HK-2 cells with ITGB6 shRNA prevented this response. (**C**) Along with the changes in surface localization of ITGB6, pretreatment of the cells with ITGB6 shRNA also inhibited the production of active TGF-β (n = 4 experiments in each group). Data are expressed as the mean ± SEM. *P < 0.0009 compared with the other 2 corresponding groups (ANOVA).

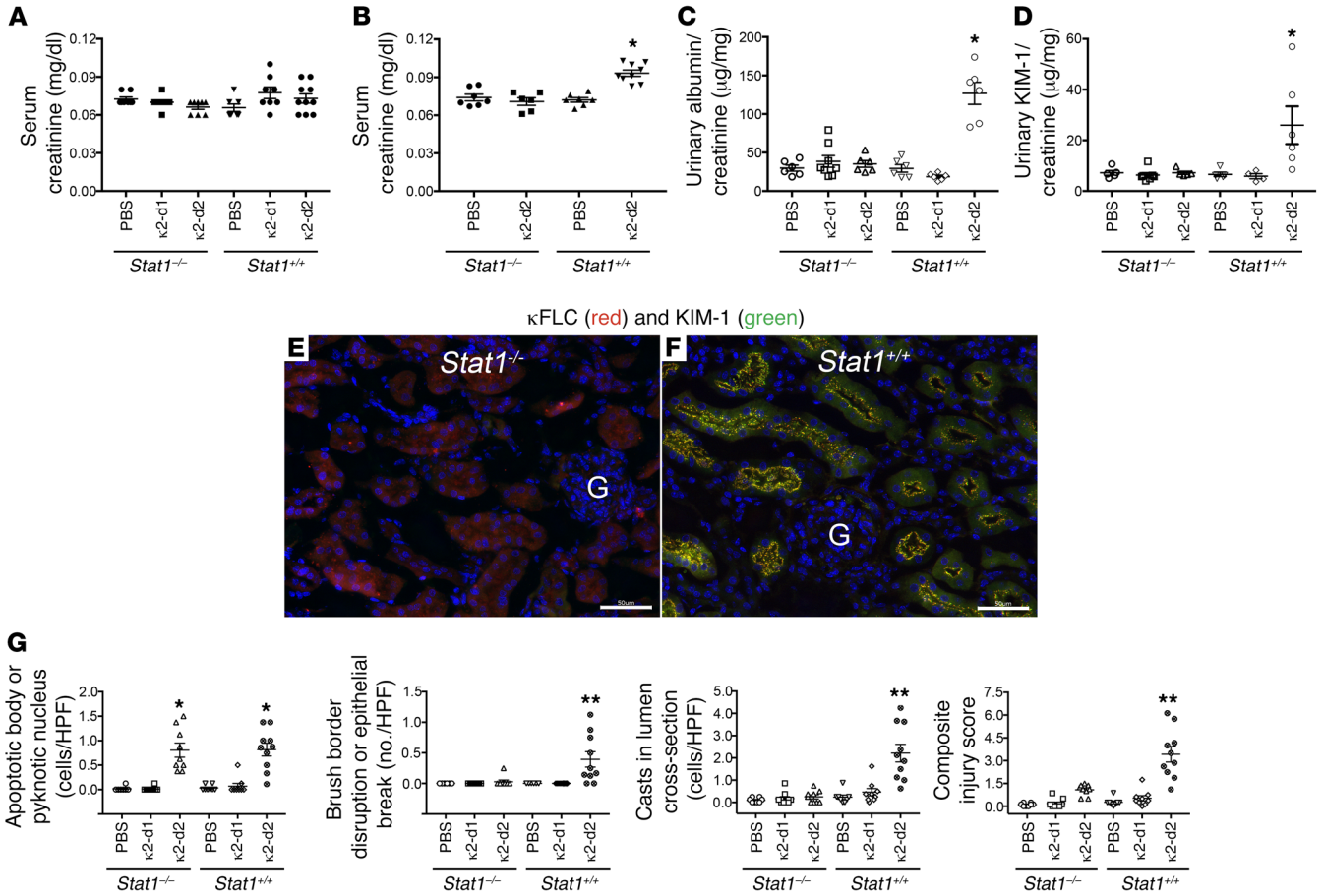

Figure 8. Effect of the 2 doses of κ2 FLCs on renal pathophysiology in *Stat1*$^{-/-}$ and *Stat1*$^{+/+}$ mice. (**A**) Mean serum creatinine concentrations (n = 9–10 mice per group) did not differ among the 6 groups on day 10. (**B**) Compared with the other 3 groups (n = 6–9 mice per group), the mean serum creatinine concentration increased specifically in the κ2-d2 group of *Stat1*$^{+/+}$ mice by day 30 of treatment. *P < 0.0001 compared with the other 4 groups (ANOVA). (**C**) Mean urinary albumin to creatinine ratios (n = 6–8 samples per group) and (**D**) mean urinary KIM-1 to creatinine ratios (n = 4–7 samples per group) were increased in the κ2-d2 group. *P < 0.01 compared with the other 4 groups (ANOVA). (**E**) Representative image of kidney cortex (n = 8–10 animals in each group) from a *Stat1*$^{-/-}$ mouse shows uptake of κ FLC into the proximal tubule (red label) but no expression of KIM-1 (green fluorescence label). (**F**) In contrast, a representative image of kidney cortex from a *Stat1*$^{+/+}$ mouse shows colocalization (yellow) of the κ FLC with KIM-1. G, glomerulus. (**G**) Blinded analysis of H&E-stained kidney tissues (n = 8–10 animals in each group) revealed an increase in injury markers: apoptotic body or pyknotic nucleus, brush border disruption or breaks in the epithelial barrier, the presence of cells in the tubular lumen, and the composite score – specifically in *Stat1*$^{+/+}$ mice treated with the higher dose of κ2 FLC. *Stat1*$^{-/-}$ mice treated with the higher dose of κ2 FLC showed a higher frequency of apoptosis markers, perhaps related to activation of other redox-sensitive pathways (19). *P < 0.0001 compared with the other 4 groups; **P < 0.0005 compared with the other 5 groups (ANOVA). Scale bars: 50 μm. All data are expressed as the mean ± SEM.

Because both the κ2 and λ3 FLCs have been well characterized and shown to produce cast nephropathy in an animal model (35), these proteins were used in the majority of the studies. All FLCs were dissolved in PBS, which served as the vehicle control in these studies.

Commercial reagents. AG-490 (30 μM, tyrphostin B42, MilliporeSigma) served as a JAK2 protein tyrosine kinase inhibitor and was dissolved in 0.03% DMSO. Ruxolitinib (LC Laboratories), a selective JAK1/2 inhibitor (27), was dissolved in 0.005% DMSO and used at a concentration of 1 μM. The solvents alone served as the corresponding vehicle controls. Next, 1,3-dimethyl-2-thiourea (DMTU) was dissolved in sterile water and added to the medium at a final concentration of 30 mM. CEA and human B2M were obtained from MilliporeSigma. Antibodies directed against total STAT1 (no. 9172); p-STAT1 (Tyr701) (D4A7); total JAK2 (D2E12); p-JAK2 (Tyr1007/1008) (C8083); p-SMAD2 (Ser465/467) (no. 3101); and p-SMAD2/3 (Ser465/467 and Ser423/425) (D27F4) were obtained from Cell Signaling Technology. Additional antibodies obtained commercially included those directed against SMAD2/3 (C4T) (MilliporeSigma); κ FLC (no. A0100, Dako, Agilent Technologies); ITGB6 (catalog TA321227, OriGene Technologies); GAPDH (catalog Ab8245, Abcam); HO-1 (ADI-SPA-894-F; Enzo Life Sciences); rat F4/80 (catalog 14480182, Invitrogen, Thermo Fisher Scientific); IL-1β (catalog Ab9722, Abcam); NIMP-R14 (sc-59338, Santa Cruz Biotechnology); and KIM-1 (AF1817, R&D Systems). LTL (FL-1321; Vector Laboratories) was used to identify the proximal tubule in the cortex and outer medulla. Secondary antibodies used for tissue immunofluorescence experiments included Alexa Fluor 594 goat anti-rabbit (catalog A11072); Alexa Fluor 488 goat anti-rabbit (catalog A11070); and Alexa Fluor 594 donkey anti-rat (catalog A21209), all from Thermo Fisher Scientific.

Commercially obtained ELISA kits included: a Human IL-1β/IL-1F2 ELISA Kit (catalog DLB50, Quantikine Immunoassay, R&D

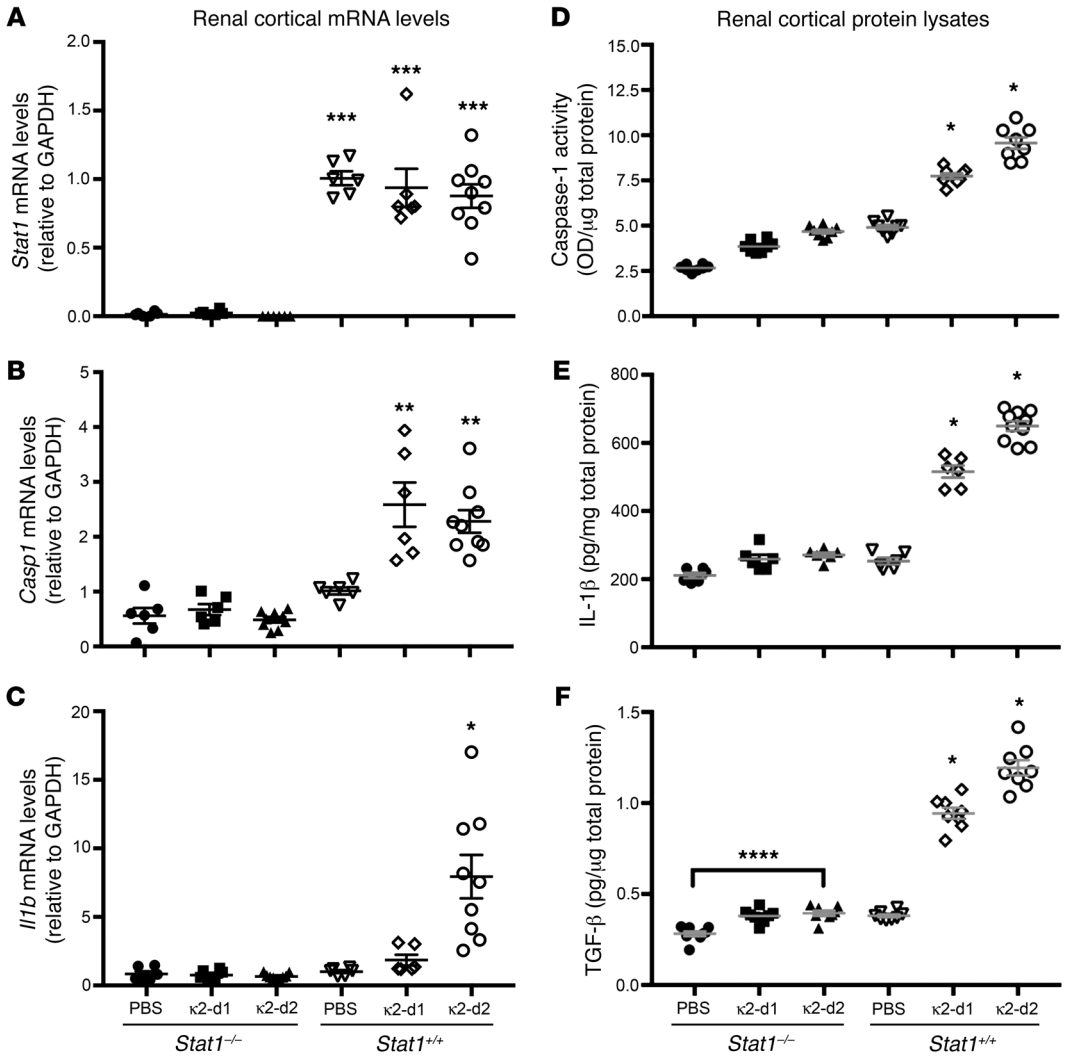

Figure 9. κ2 FLC increases in vivo steady-state mRNA levels of *Casp1* and *Il1b* and produces dose-dependent increases in caspase-1 activity and IL-1β and TGF-β expression in cortical lysates of *Stat1*$^{+/+}$, but not *Stat1*$^{-/-}$, mice. n = 6–10 animals per group. (**A**) Renal cortical steady-state *Stat1* mRNA confirmed the absence of *Stat1* in the kidneys of *Stat1*$^{-/-}$ mice and no differences among the *Stat1*$^{+/+}$ mice (n = 6–9 samples/group). (**B**) *Casp1* mRNA increased in the kidney cortex of *Stat1*$^{+/+}$ mice treated with both doses of the κ2 FLCs (n = 6–9 samples/group). (**C**) *Il1b* mRNA increased in the κ2-d2–treated *Stat1*$^{+/+}$ mice (n = 6–9 samples/group). Treatment of *Stat1*$^{+/+}$ mice with both doses of the κ2 FLCs increased (**D**) caspase-1 activity (n = 8 samples/group); (**E**) IL-1β expression (n = 6–10 samples/group); and (**F**) active TGF-β expression (n = 7–8 samples/group) in the cortical lysates of *Stat1*$^{+/+}$ mice treated with both doses of the κ2 FLCs. Data are expressed as the mean ± SEM. *P < 0.0005 compared with the other 5 groups; **P < 0.0005 compared with *Stat1*$^{-/-}$ mice treated with PBS, κ2-d1, and κ2-d2 and compared with *Stat1*$^{+/+}$ mice treated with PBS; ***P < 0.0001 compared with *Stat1*$^{-/-}$ mice. A small but significant increase in active TGF-β expression was observed in cortical lysates of *Stat1*$^{-/-}$ mice treated with the higher dose of the κ2 FLC when compared with *Stat1*$^{-/-}$ mice treated with vehicle (PBS) alone; ****P = 0.0192. (ANOVA for all.)

Systems); a Mouse IL-1β ELISA Kit (catalog RAB0275, Millipore-Sigma); a Caspase-1 Colorimetric Assay Kit (Ab39470, Abcam) or a Caspase-1 Fluorometric Assay Kit (Ab39412, Abcam); a Mouse TGF-β1 ELISA Kit (catalog LS-F5184-1, LifeSpan BioSciences); a Mouse Albumin ELISA Kit (catalog E99134, Bethyl Laboratories); and a Mouse TIM-1/KIM-1/HAVCR1 ELISA Kit (catalog MKM100, R&D Systems).

siRNA designed to target human STAT1 (3 unique 27-mer siRNA duplexes, locus ID 6772) and nontargeting siRNA (Trilencer-27 Universal Scrambled Negative Control siRNA, SR30004) were obtained from OriGene Technologies. ITGB6 was knocked down using shRNA (ITGB6 Human shRNA Plasmid Kit Locus ID 3694, OriGene Technologies), with a nontargeting shRNA (TR30015, OriGene Technologies) serving as a control.

We also used a recombinant κII subfamily FLC, which was synthesized at the Recombinant Protein Expression and Purification Core directed by Zhirui Wang at Harvard Medical School (Boston, Massachusetts, USA). After obtaining the protein sequence, production of the protein proceeded in standard fashion (61–63). Briefly, the codon sequence was optimized for expression in *Pichia pasoris*. Following synthesis and confirmation of the entire codon-optimized sequence and cloning into a yeast expression vector, the yeast were transformed, and the recombinant protein was expressed and secreted into the medium, permitting purification. A 6× His tag was added to facilitate purification. Because the initial recombinant protein identified an N-linked glycosylation site in the CDR1 domain, the amino acid sequence was modified by replacing the asparagine with the aspartic acid, which eliminated the

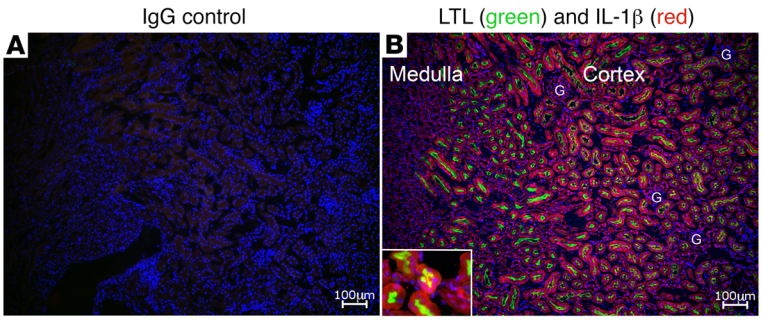

Figure 10. The proximal tubules of *Stat1*$^{+/+}$ mice produce IL-1β following treatment with the higher dose of κ2 FLC. (**A**) The IgG control showed minimal background staining of the tubules. (**B**) Representative images show production of IL-1β (red fluorescence) colocalized with tubules (n = 8–10 animals in each group) that also stained with LTL. Inset is a higher-magnification image showing colocalization of LTL, which labeled the apical side of proximal tubule cells, with IL-1β in the cytoplasm. Scale bars: 100 μm. Original magnification ×1200.

glycosylation site. Subsequent purification of this V_L and another recombinant protein that had an identical sequence except for a W40G substitution (mutant V_L) produced the desired purity (Figure 5).

Animal and tissue preparation

Colonies of *Stat1*-knockout mice (termed *Stat1*$^{-/-}$ mice) and littermate controls (termed *Stat*$^{+/+}$ mice) were developed and confirmed by PCR-based genotyping (Supplemental Table 3, Supplemental Figure 1, and Supplemental Figure 2) and maintained in a gnotobiotic facility. Studies were conducted using 26 *Stat*$^{+/+}$ and 26 *Stat1*$^{-/-}$ mice. All animal studies were conducted using animal biosafety level 3 laboratory and Sealsafe cages with HEPA filters, and personnel wore personal protective equipment. *Stat1*$^{-/-}$ mice grew normally and were phenotypically normal under these conditions.

At the start of the experiment, 8-week-old male *Stat1*$^{+/+}$ and *Stat1*$^{-/-}$ mice (n = 8–10/group) were intraperitoneally injected daily with either PBS alone (Invitrogen, Thermo Fisher Scientific) as a vehicle or with a lower dose (termed κ2-d1) (0.033 mg/g BW) or higher dose (termed κ2-d2) (0.165 mg/g BW) of κ2 FLC in PBS. The experiments were concluded on day 10 or day 30. Serum was collected for creatinine measurement, which was done using liquid chromatography tandem mass spectrometry (Waters 2795 LC-MS/MS, Waters Corp.), and urine was collected to determine albumin and KIM-1 levels, since increased urinary excretion of albumin and KIM-1 is a sensitive biomarker of tubular injury (37–39). The left kidney was harvested for histological and immunohistochemical analyses, and the right kidney cortex was harvested for immunoblotting, ELISA, and real-time RT-PCR.

Kidneys were fixed in 10% neutral buffered formalin (catalog SF100-4, Thermo Fisher Scientific) overnight, and embedded tissue was sectioned at 5-μm thickness for histological staining. H&E staining was performed at the University of Alabama at Birmingham Comparative Pathology Laboratory, and stained sections were imaged and analyzed by light microscopy at ×40 magnification (model DMI6000 B, Leica). Morphological analysis was conducted using 7–9 images of H&E-stained sections from each animal. The number of pyknotic nuclei within cells per high-powered field (HPF) was quantified. Brush border loss and the presence of casts, either proteinaceous or cellular in nature, were evaluated as the number of tubule cross-sections per HPF. A composite injury score was produced by summing each of the 3 markers of injury. For quantification of tubulointerstitial

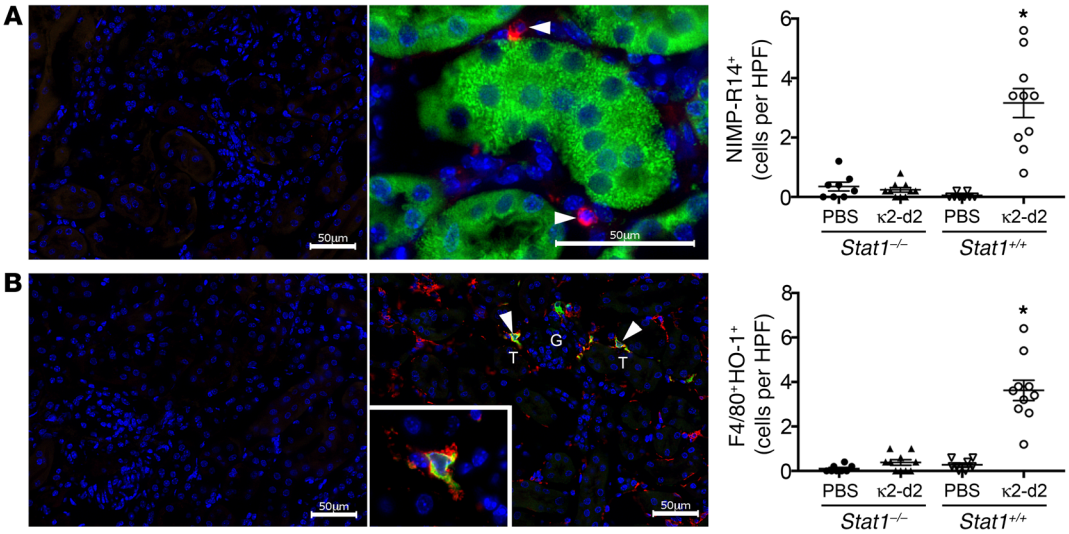

Figure 11. FLCs induce a peritubular inflammatory infiltrate that includes neutrophils and F4/80$^+$HO-1$^+$ macrophages. (**A**) Neutrophils, detected using anti–NIMP-R14 antibodies (red fluorescence), were present in greater numbers (white arrowheads) only in the *Stat1*$^{+/+}$ mice treated with the higher dose of κ2 FLC. Proximal tubule expression of ITGB6 (green fluorescence) was readily detected. The IgG controls (left panel) showed minimal background staining of the samples. (**B**) M2 macrophage numbers, detected by colocalization of F4/80 (red fluorescence) with HO-1 (green fluorescence), were increased (white arrowheads) only in the *Stat1*$^{+/+}$ mice treated with κ2 FLC. The inset shows a magnified image of a F4/80$^+$HO-1$^+$ cell (colocalized stain is shown in yellow). The IgG controls (left panel) showed minimal background staining of the samples. T, tubule. n = 8–10 mice/group. Data are expressed as the mean ± SEM of cells per HPF. *P < 0.0001 compared with the other 3 groups (ANOVA). Scale bars: 50 μm. Original magnification ×1200.

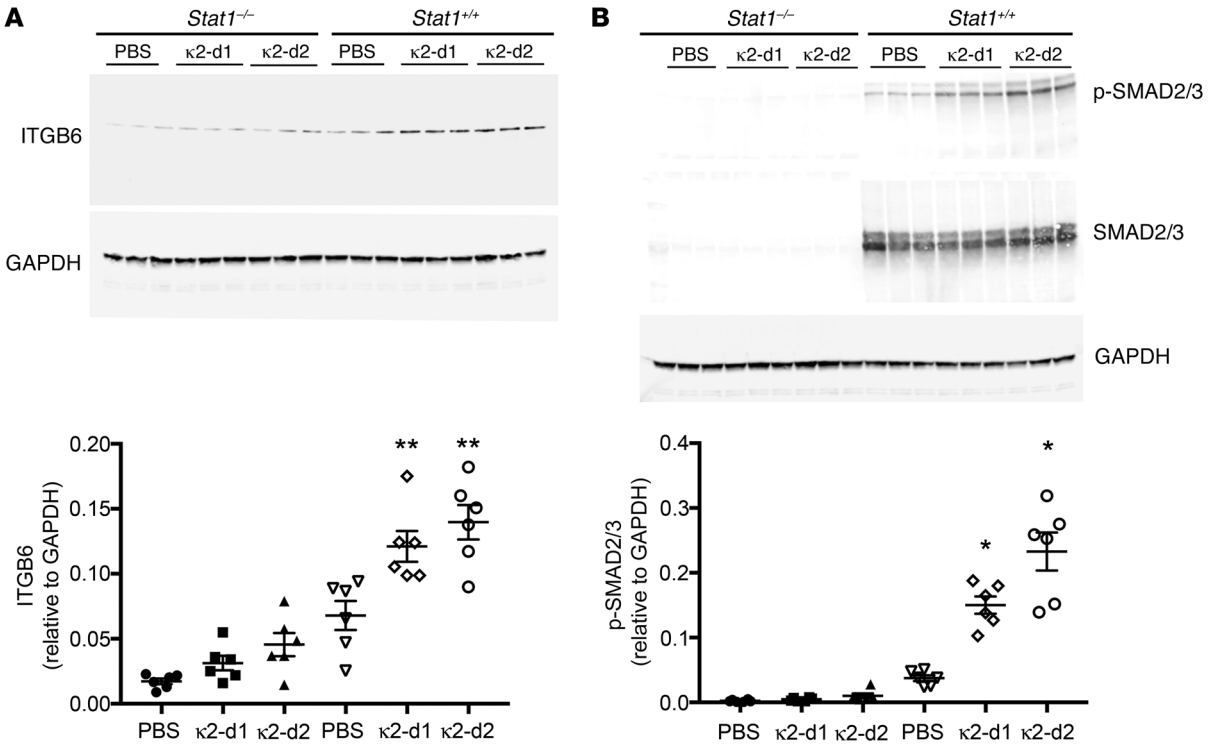

Figure 12. Treatment of *Stat1*$^{+/+}$ mice with κ2 FLC promotes an increase in ITGB6 and p-SMAD2/3 in the kidney cortex. (**A**) Both doses of the κ2 FLCs prompted increases in ITGB6 levels of cortical lysates from *Stat1*$^{+/+}$ mice (n = 6 mice/group). Data are expressed as the mean ± SEM. $^{**}P \leq 0.006$ compared with each of the other 4 groups (ANOVA). Relative ITGB6 levels were greater ($P = 0.0096$, ANOVA) in the PBS-treated *Stat1*$^{+/+}$ mice compared with levels in the PBS-treated *Stat1*$^{-/-}$ mice. (**B**) A dose-dependent effect of κ2 FLC on p-SMAD2/3 was observed in *Stat1*$^{+/+}$ mice but produced no changes in p-SMAD2/3 in *Stat1*$^{-/-}$ mice. Because SMAD2/3 levels were remarkably low in the kidney cortex of *Stat1*$^{-/-}$ mice, the data were factored by the density of GAPDH in the samples. n = 6 mice/group. Data are expressed as the mean ± SEM. $^{*}P < 0.005$ compared with each of the other 5 groups in the experiment (ANOVA).

erstitial fibrosis, 5-μm-thick sections were stained with Picrosirius red using the NovaUltra Picrosirius Red Stain Kit (catalog IW-3012, IHC World). Stained sections were imaged at ×40 magnification using polarized microscopy (model BX43F, Olympus) and analyzed with ImageJ, version 1.51 (NIH).

Immunofluorescence microscopy of kidney tissues

Kidneys (n = 8–10 animals in each group) were fixed in 4% paraformaldehyde overnight and cryopreserved in 20% sucrose. Embedded tissue was sectioned at 5-μm thickness and underwent standard antigen retrieval methods that included pretreatment with 70% ethanol at –20°C for 10 minutes (macrophage, FLC and KIM-1 staining), 0.1% SDS in PBS for 5 minutes (ITGB6 and neutrophil staining), and acetone at –20°C for 2 minutes (IL-1β staining). Autofluorescence was reduced by incubation in 50 mM ammonium chloride in PBS for 15 minutes. Nonspecific staining in the sections was blocked by incubation in 2% normal horse serum in PBS for 1 hour, followed by incubation with specific primary antibodies overnight at 4°C. Nuclei were identified using a DAPI label in the mounting media (catalog H-1500, VectaShield, Vector Laboratories). Negative controls for each experiment included staining with IgG of the corresponding species (catalog I-1000, lot X0112, and catalog I-5000, lot X0404, Vector Laboratories; and catalog 559478, BD Pharmingen) and no primary antibody. Positive controls for the experiments included splenic tissue for macrophage and neutrophil staining and ischemia-reperfusion injury tissue for KIM-1 staining (data not shown). The stained sections were viewed by epifluorescence microscopy (model BZ-X800, Keyence).

To quantify macrophages and neutrophils, stained sections were imaged at ×400 magnification. Five representative images were used to obtain the counts. The cells that colocalized with HO-1 and F4/80 stains were counted as activated macrophages. Likewise, cells positive for NIMP-R14 staining were counted in each image taken. The average numbers of cells per HPF were determined for each animal.

Determination of FLC-mediated production of H_2O_2

Experiments were performed as described previously (18). Briefly, 100 μl of sample FLCs or purified recombinant κII V_L and mutant κII V_L, 3 μM in PBS, in a sealed glass container was exposed to near-UV radiation (312 nm, 800 μWcm^{-2}) for 1, 3, and 6 hours, using an Electronic Dual-Light Transilluminator (Ultra-Lum Inc.). Experimental controls included samples that were not exposed to near-UV radiation and CEA and human B2M. B2M was used as a control because it is a circulating low-molecular-weight protein that has a 3D structure that resembles an immunoglobulin constant domain (64). H_2O_2 production was determined using an Amplex Red Hydrogen Peroxide/Peroxidase Assay Kit (Molecular Probes). Treated samples and standards were mixed with Amplex Red working solution and incubated at room temperature for 30 minutes, protected from light. Fluorescence emission excited at 535 nm was detected at 560 nm (VersaMax Microplate Reader, Molecular Devices). All samples were tested in duplicate and averaged.

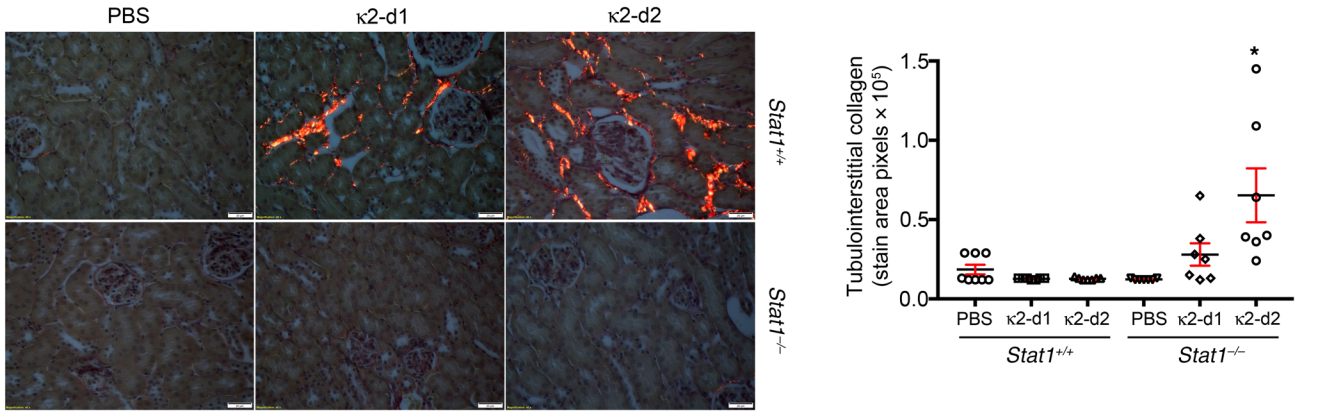

Figure 13. Treatment of *Stat1*$^{+/+}$ mice with κ2 FLC promotes increased interstitial collagen deposition. *Stat1*$^{+/+}$ mice treated with κ2 FLC had increased interstitial collagen deposition (red and yellow colors), detected using Picrosirius red, in the kidney cortex. In contrast, *Stat1*$^{-/-}$ mice did not have deposition of collagen following exposure to either dose of the FLC. n = 7–8 mice in each group. Scale bars: 20 μm. *P < 0.0001 compared with the other 5 groups in the experiment (ANOVA).

In other experiments, the production of H_2O_2 in the medium was determined following incubation of confluent HK-2 cells with monoclonal FLC and recombinant proteins. In these studies, the medium was exchanged with K-SFM that contained the FLC (1 mg/ml), CEA (15 mg/ml), B2M (1 mg/ml), or purified κII V_L and mutant κII V_L (0.5 mg/ml). Incubation continued for 24 hours at 37°C. The medium was harvested, and H_2O_2 was quantified using the commercial assay.

For immunofluorescence studies, 5 minutes before the end of the incubation period, HK-2 cells were incubated in HBSS that contained 5-(and-6)-carboxy-2′,7′-dichlorodihydrofluorescein diacetate (carboxy-H2DCFDA, Image-iT LIVE Green Reactive Oxygen Species Detection Kit, Molecular Probes), a reliable fluorogenic marker for ROS, following the protocol provided by the manufacturer. Cells were counterstained with Hoechst, washed, mounted, and imaged immediately using confocal laser scanning microscopy (model LSM 710 confocal microscope, Carl Zeiss Microimaging) provided by the High-Resolution Imaging Facility at the University of Alabama at Birmingham.

Real-time RT-PCR analysis of mRNA expression

Total RNA was extracted from kidney cortex with TRIzol (Invitrogen, Thermo Fisher Scientific) and treated with DNAase I to remove genomic DNA and then purified with the use of an RNA purification kit (catalog 12183025, Invitrogen, Thermo Fisher Scientific). The DNA-free RNA was reverse transcribed to cDNA with the use of the SuperScript IV RT Kit (catalog 18091050, Invitrogen, Thermo Fisher Scientific). cDNA was amplified with SYBR Green PCR in the LightCycler 480 system (Roche Diagnostics) and with specific primers (Supplemental Table 2) for 40 cycles. Steady-state mRNA levels were calculated according to the threshold cycle generated with the LightCycler 480 software. Relative mRNA expression was normalized to GAPDH.

Determination of IL-1β, TGF-β, and caspase-1 activity

At the start of the experiment, cell culture medium was exchanged for K-SFM containing vehicle or FLCs (1 mg/ml) or purified recombinant κII V_L and mutant κII V_L (0.5 mg/ml), with or without 30 μM AG-490. Incubation continued overnight, and the medium was harvested promptly for assays. Cells were collected and lysed in RIPA buffer for Western blot analyses, or in lysis buffer from ELISA kits containing a protease inhibitor cocktail (cOmplete, Roche). For the in vivo studies, the kidney cortex was homogenized in RIPA buffer or lysis buffer from ELISA kits. Cell supernatants and cell or tissue lysates were clarified by centrifugation and stored at –70°C until assayed. Total soluble protein in lysates was determined using a BCA Protein Assay Kit (Pierce, Thermo Fisher Scientific). An enzyme immunoassay for the quantitative determination of IL-1β proceeded in standard fashion, following the manufacturer's directions, using 200 μl of the sample. Absorbance was determined at 450 nm (VersaMax Microplate Reader, Molecular Devices). Assays were performed in duplicate and averaged. The levels of total and active TGF-β in the cell culture medium were quantified as done previously using a plasminogen activator inhibitor-1 lucif-

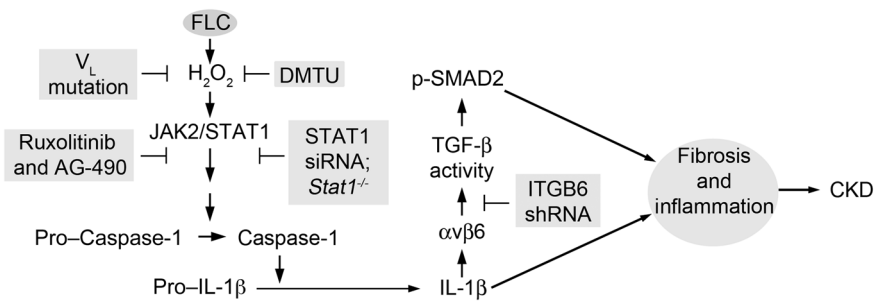

Figure 14. Summary of the findings of this study. This study demonstrated that monoclonal FLCs can produce events in the proximal tubule that lead to chronic kidney disease (CKD).

erase reporter assay in mink lung epithelial cells (65). Active TGF-β in mouse kidney lysates was quantified using a Mouse TGF-β1 ELISA Kit (LifeSpan BioSciences).

Caspase-1 activity in HK-2 cells was determined in 50 μl cell lysates produced using chilled lysis buffer from the kit. For the in vivo experiments, kidney cortex was homogenized in lysis buffer from the kit, and 50 μl of the lysate was assayed following the manufacturer's instructions. Assays were performed in duplicate, with the averages taken. The results were factored by the amount of total protein in the lysates.

Western blot analyses

Tissue and cell lysates were produced using modified RIPA buffer that contained 10 mM Tris-HCl, pH 7.4, 100 mm NaCl, 1 mM EDTA, 1 mM EGTA, 0.5% sodium deoxycholate, 1% Triton X-100, 10% glycerol, 0.1% SDS, 20 mM sodium pyrophosphate, 2 mM Na_3VO_4, 1 mM NaF, 1 mM PMSF, and a protease inhibitor cocktail. Total protein concentration was determined using a BCA Protein Assay Reagent Kit (Pierce Protein Research Products, Thermo Fisher Scientific). Protein extracts (20–60 μg) were boiled for 3 minutes in Laemmli buffer and separated by 7% to 12% SDS-PAGE (Bio-Rad Laboratories), before electrophoretic transfer onto PVDF membranes. The membranes were blocked in 5% nonfat milk and then probed with an antibody (diluted 1:1000) that recognized specifically STAT1 and p-STAT1, JAK2 and p-JAK2, SMAD2/3 and p-SMAD2 or p-SMAD2/3, ITGB6, and GAPDH. After the washes, the blots were incubated for 1 hour at room temperature with Alexa Fluor 680– or 790–conjugated AffiniPure secondary antibody (1:10,000 dilution). The bands were detected using the Odyssey Infrared Imaging System (LI-COR Biosciences), and densitometric analysis was performed using Image Studio Software (LI-COR Biosciences).

Silencing of STAT1 and response to FLCs

HK-2 cells at 70% confluence were transfected using siRNA transfection reagent (DharmaFECT1, Dharmacon RNA Technologies) containing varying amounts (0–100 nmol/l) of siRNA. Preliminary experiments that used the siTOX transfection control (Dharmacon RNA Technologies) determined the optimum exposure conditions that maximized transfection efficiency and minimized toxicity. STAT1 siRNA (50 nmol/l) was complexed with 2 μl DharmaFECT1 in 200 μl total volume and then added to complete medium in a final volume of 1 ml for each well in a 12-well plate. After incubation in the transfection solution for 12 hours, the medium was refreshed and incubation continued up to 48 hours. The cells were then incubated for an additional 24 hours in medium containing 1 mg/ml FLCs, 0.5 mg/ml recombinant κII V_L and mutant κII V_L, and vehicle. Medium or cell lysates were harvested for determination of STAT1, p-STAT1 (Y701), SMAD2/3, p-SMAD2 (S465/7), caspase-1 activity, IL-1β, and total and active TGF-β.

Silencing of ITGB6 and response to FLCs

HK-2 cells at 70% confluence were transfected using siTRAN 1.0 transfection reagent (OriGene Technologies) containing shRNA targeting ITGB6 or a nontargeting shRNA. The shRNA mix (500 ng each) was complexed with 60 μl siTRAN 1.0 in 150 μl total volume and added to the complete medium in a final volume of 3 ml for each well in a 6-well plate. After incubation in the transfection solution for 48 hours, the medium was replaced, and cells transfected with ITGB6D shRNA or control shRNA were incubated in medium containing 1 mg/ml FLCs or vehicle for an additional 24 hours before collecting the medium and cells for FACS.

FACS was used to quantify cell-surface labeling of ITGB6. The harvested cells were washed twice with ice-cold PBS and once with staining buffer and then resuspended in 100 μl/10^6 cells/tube and blocked in staining buffer for 10 minutes at 4°C. The cellular pellet was stained with 100 μl buffer containing anti–ITGB6 rabbit monoclonal antibody (catalog 187155, Abcam) at 0.1 μg/10^6 cells. After a 60-minute incubation at 4°C, the cells were washed with cold staining buffer, resuspended in 100 μl annexin binding buffer with 0.2 μg/ml Alexa Fluor 488 F(ab′) antibody fragment (catalog A11070, Invitrogen, Thermo Fisher Scientific), and incubated for 30 minutes at 4°C. Fluorescence was acquired using a BD FACSCalibur Flow Cytometer. Data were analyzed with CellQuest software (BD Biosciences).

Statistics

All data are expressed as the mean ± SEM. For multiple group comparisons, either ANOVA or factorial ANOVA, followed by Tukey's multiple comparisons test, was performed. A P value of less than 0.05 was considered statistically significant.

Study approval

This study was carried out in strict accordance with the recommendations in the NIH's *Guide for the Care and Use of Laboratory Animals* (National Academies Press, 2011). The IACUC of the University of Alabama at Birmingham approved the project. The IRB of the Birmingham Department of Veterans Affairs provided annual continuing oversight and approval of this research activity.

Author contributions

PWS conceived the study. WWY, XL, SR, WF, and PWS designed the study. WWY, XL, SR, WF, LMC, and PWS performed the experiments and/or analyzed the data. All authors participated in writing and editing the manuscript.

Acknowledgments

This work was supported by a Merit Award (1 I01 CX001326) from the United States Department of Veterans Affairs Clinical Sciences R&D (CSRD) Service; a NIH George M. O'Brien Kidney and Urological Research Centers Program grant (P30 DK079337); and an Anderson Innovation Award.

Address correspondence to: Paul W. Sanders, Division of Nephrology/Department of Medicine, 642 Lyons-Harrison Research Building, 1530 Third Avenue, South, University of Alabama at Birmingham, Birmingham, Alabama 35294-0007, USA. Phone: 205.934.3589; E-mail: psanders@uabmc.edu.

1. Jemal A, Siegel R, Xu J, Ward E. Cancer statistics, 2010. *CA Cancer J Clin*. 2010;60(5):277–300.
2. Kyle RA, et al. Review of 1027 patients with newly diagnosed multiple myeloma. *Mayo Clin Proc*. 2003;78(1):21–33.
3. Dimopoulos MA, et al. Significant improvement in the survival of patients with multiple myeloma presenting with severe renal impairment after the introduction of novel agents. *Ann Oncol*. 2014;25(1):195–200.
4. Bladé J, et al. Renal failure in multiple myeloma: presenting features and predictors of outcome in

94 patients from a single institution. *Arch Intern Med*. 1998;158(17):1889–1893.
5. Reule S, Sexton DJ, Solid CA, Chen SC, Foley RN. ESRD due to Multiple Myeloma in the United States, 2001-2010. *J Am Soc Nephrol*. 2016;27(5):1487–1494.
6. Knudsen LM, Hjorth M, Hippe E. Renal failure in multiple myeloma: reversibility and impact on the prognosis. Nordic Myeloma Study Group. *Eur J Haematol*. 2000;65(3):175–181.
7. Iványi B. Frequency of light chain deposition nephropathy relative to renal amyloidosis and Bence Jones cast nephropathy in a necropsy study of patients with myeloma. *Arch Pathol Lab Med*. 1990;114(9):986–987.
8. Herrera GA, Joseph L, Gu X, Hough A, Barlogie B. Renal pathologic spectrum in an autopsy series of patients with plasma cell dyscrasia. *Arch Pathol Lab Med*. 2004;128(8):875–879.
9. Hutchison CA, et al. Early reduction of serum-free light chains associates with renal recovery in myeloma kidney. *J Am Soc Nephrol*. 2011;22(6):1129–1136.
10. Ludwig H, et al. Light chain-induced acute renal failure can be reversed by bortezomib-doxorubicin-dexamethasone in multiple myeloma: results of a phase II study. *J Clin Oncol*. 2010;28(30):4635–4641.
11. Dimopoulos MA, et al. VMP (Bortezomib, Melphalan, and Prednisone) is active and well tolerated in newly diagnosed patients with multiple myeloma with moderately impaired renal function, and results in reversal of renal impairment: cohort analysis of the phase III VISTA study. *J Clin Oncol*. 2009;27(36):6086–6093.
12. Dimopoulos MA, et al. Reversibility of renal impairment in patients with multiple myeloma treated with bortezomib-based regimens: identification of predictive factors. *Clin Lymphoma Myeloma*. 2009;9(4):302–306.
13. Dimopoulos MA, et al. The role of novel agents on the reversibility of renal impairment in newly diagnosed symptomatic patients with multiple myeloma. *Leukemia*. 2013;27(2):423–429.
14. Gonsalves WI, et al. Improvement in renal function and its impact on survival in patients with newly diagnosed multiple myeloma. *Blood Cancer J*. 2015;5:e296.
15. Roussou M, et al. Reversibility of renal failure in newly diagnosed patients with multiple myeloma and the role of novel agents. *Leuk Res*. 2010;34(10):1395–1397.
16. Scheid C, et al. Bortezomib before and after autologous stem cell transplantation overcomes the negative prognostic impact of renal impairment in newly diagnosed multiple myeloma: a subgroup analysis from the HOVON-65/GMMG-HD4 trial. *Haematologica*. 2014;99(1):148–154.
17. Basnayake K, et al. Resolution of cast nephropathy following free light chain removal by haemodialysis in a patient with multiple myeloma: a case report. *J Med Case Rep*. 2008;2:380.
18. Wang PX, Sanders PW. Immunoglobulin light chains generate hydrogen peroxide. *J Am Soc Nephrol*. 2007;18(4):1239–1245.
19. Ying WZ, Wang PX, Sanders PW. Pivotal role of apoptosis signal-regulating kinase 1 in monoclonal free light chain-mediated apoptosis. *Am J Pathol*. 2012;180(1):41–47.
20. Ying WZ, Wang PX, Aaron KJ, Basnayake K, Sanders PW. Immunoglobulin light chains activate nuclear factor-κB in renal epithelial cells through a Src-dependent mechanism. *Blood*. 2011;117(4):1301–1307.
21. Basnayake K, Ying WZ, Wang PX, Sanders PW. Immunoglobulin light chains activate tubular epithelial cells through redox signaling. *J Am Soc Nephrol*. 2010;21(7):1165–1173.
22. Brenner DA, et al. Human amyloidogenic light chains directly impair cardiomyocyte function through an increase in cellular oxidant stress. *Circ Res*. 2004;94(8):1008–1010.
23. Diomede L, et al. A Caenorhabditis elegans-based assay recognizes immunoglobulin light chains causing heart amyloidosis. *Blood*. 2014;123(23):3543–3552.
24. Shi J, et al. Amyloidogenic light chains induce cardiomyocyte contractile dysfunction and apoptosis via a non-canonical p38alpha MAPK pathway. *Proc Natl Acad Sci U S A*. 2010;107(9):4188–4193.
25. Sanders PW. Mechanisms of light chain injury along the tubular nephron. *J Am Soc Nephrol*. 2012;23(11):1777–1781.
26. Meydan N, et al. Inhibition of acute lymphoblastic leukaemia by a Jak-2 inhibitor. *Nature*. 1996;379(6566):645–648.
27. Quintás-Cardama A, et al. Preclinical characterization of the selective JAK1/2 inhibitor INCB018424: therapeutic implications for the treatment of myeloproliferative neoplasms. *Blood*. 2010;115(15):3109–3117.
28. Ramakrishnan V, et al. TG101209, a novel JAK2 inhibitor, has significant in vitro activity in multiple myeloma and displays preferential cytotoxicity for CD45+ myeloma cells. *Am J Hematol*. 2010;85(9):675–686.
29. Sengul S, Zwizinski C, Simon EE, Kapasi A, Singhal PC, Batuman V. Endocytosis of light chains induces cytokines through activation of NF-kappaB in human proximal tubule cells. *Kidney Int*. 2002;62(6):1977–1988.
30. Sengul S, Zwizinski C, Batuman V. Role of MAPK pathways in light chain-induced cytokine production in human proximal tubule cells. *Am J Physiol Renal Physiol*. 2003;284(6):F1245–F1254.
31. Biasini M, et al. SWISS-MODEL: modelling protein tertiary and quaternary structure using evolutionary information. *Nucleic Acids Res*. 2014;42(Web Server issue):W252–W258.
32. Arnold K, Bordoli L, Kopp J, Schwede T. The SWISS-MODEL workspace: a web-based environment for protein structure homology modelling. *Bioinformatics*. 2006;22(2):195–201.
33. Bienert S, et al. The SWISS-MODEL Repository-new features and functionality. *Nucleic Acids Res*. 2017;45(D1):D313–D319.
34. Kiefer F, Arnold K, Künzli M, Bordoli L, Schwede T. The SWISS-MODEL Repository and associated resources. *Nucleic Acids Res*. 2009;37(Database issue):D387–D392.
35. Ying WZ, Allen CE, Curtis LM, Aaron KJ, Sanders PW. Mechanism and prevention of acute kidney injury from cast nephropathy in a rodent model. *J Clin Invest*. 2012;122(5):1777–1785.
36. Kusaba T, Lalli M, Kramann R, Kobayashi A, Humphreys BD. Differentiated kidney epithelial cells repair injured proximal tubule. *Proc Natl Acad Sci USA*. 2014;111(4):1527–1532.
37. Ware LB, Johnson AC, Zager RA. Renal cortical albumin gene induction and urinary albumin excretion in response to acute kidney injury. *Am J Physiol Renal Physiol*. 2011;300(3):F628–F638.
38. Han WK, Bailly V, Abichandani R, Thadhani R, Bonventre JV. Kidney injury molecule-1 (KIM-1): a novel biomarker for human renal proximal tubule injury. *Kidney Int*. 2002;62(1):237–244.
39. Bonventre JV. Kidney injury molecule-1 (KIM-1): a urinary biomarker and much more. *Nephrol Dial Transplant*. 2009;24(11):3265–3268.
40. Sierra-Filardi E, Vega MA, Sánchez-Mateos P, Corbí AL, Puig-Kröger A. Heme oxygenase-1 expression in M-CSF-polarized M2 macrophages contributes to LPS-induced IL-10 release. *Immunobiology*. 2010;215(9-10):788–795.
41. Braga TT, Agudelo JS, Camara NO. Macrophages during the fibrotic process: M2 as friend and foe. *Front Immunol*. 2015;6:602.
42. March CJ, et al. Cloning, sequence and expression of two distinct human interleukin-1 complementary DNAs. *Nature*. 1985;315(6021):641–647.
43. LeBleu VS, et al. Origin and function of myofibroblasts in kidney fibrosis. *Nat Med*. 2013;19(8):1047–1053.
44. Lemos DR, et al. Interleukin-1. *J Am Soc Nephrol*. 2018;29(6):1690–1705.
45. Datta D, Vaidehi N, Xu X, Goddard WA. Mechanism for antibody catalysis of the oxidation of water by singlet dioxygen. *Proc Natl Acad Sci U S A*. 2002;99(5):2636–2641.
46. Wentworth AD, Jones LH, Wentworth P, Janda KD, Lerner RA. Antibodies have the intrinsic capacity to destroy antigens. *Proc Natl Acad Sci U S A*. 2000;97(20):10930–10935.
47. Wentworth P, et al. Antibody catalysis of the oxidation of water. *Science*. 2001;293(5536):1806–1811.
48. Wentworth P, et al. Evidence for the production of trioxygen species during antibody-catalyzed chemical modification of antigens. *Proc Natl Acad Sci U S A*. 2003;100(4):1490–1493.
49. Zhu X, Wentworth P, Wentworth AD, Eschenmoser A, Lerner RA, Wilson IA. Probing the antibody-catalyzed water-oxidation pathway at atomic resolution. *Proc Natl Acad Sci U S A*. 2004;101(8):2247–2252.
50. Madamanchi NR, Li S, Patterson C, Runge MS. Reactive oxygen species regulate heat-shock protein 70 via the JAK/STAT pathway. *Arterioscler Thromb Vasc Biol*. 2001;21(3):321–326.
51. Simon AR, Rai U, Fanburg BL, Cochran BH. Activation of the JAK-STAT pathway by reactive oxygen species. *Am J Physiol*. 1998;275(6):C1640–C1652.
52. Guo H, Callaway JB, Ting JP. Inflammasomes: mechanism of action, role in disease, and therapeutics. *Nat Med*. 2015;21(7):677–687.
53. Anders HJ, Muruve DA. The inflammasomes in kidney disease. *J Am Soc Nephrol*. 2011;22(6):1007–1018.
54. Pittet JF, et al. HMGB1 accelerates alveolar epithelial repair via an IL-1β- and αvβ6 integrin-dependent activation of TGF-β1. *PLoS ONE*. 2013;8(5):e63907.
55. Ma LJ, et al. Transforming growth factor-beta-dependent and -independent pathways of induction of tubulointerstitial fibrosis in beta6(-/-)

mice. *Am J Pathol*. 2003;163(4):1261–1273.
56. Hahm K, et al. Alphav beta6 integrin regulates renal fibrosis and inflammation in Alport mouse. *Am J Pathol*. 2007;170(1):110–125.
57. Puthawala K, et al. Inhibition of integrin alpha(v) beta6, an activator of latent transforming growth factor-beta, prevents radiation-induced lung fibrosis. *Am J Respir Crit Care Med*. 2008;177(1):82–90.
58. Munger JS, et al. The integrin alpha v beta 6 binds and activates latent TGF beta 1: a mechanism for regulating pulmonary inflammation and fibrosis. *Cell*. 1999;96(3):319–328.
59. Gewin L, Zent R, Pozzi A. Progression of chronic kidney disease: too much cellular talk causes damage. *Kidney Int*. 2017;91(3):552–560.
60. Ryan MJ, Johnson G, Kirk J, Fuerstenberg SM, Zager RA, Torok-Storb B. HK-2: an immortalized proximal tubule epithelial cell line from normal adult human kidney. *Kidney Int*. 1994;45(1):48–57.
61. Peraino J, et al. Expression and purification of soluble porcine CTLA-4 in yeast Pichia pastoris. *Protein Expr Purif*. 2012;82(2):270–278.
62. Hermanrud CE, et al. Expression and purification of non-N-glycosylated porcine interleukin 3 in yeast Pichia pastoris. *Protein Expr Purif*. 2012;82(1):70–74.
63. Peraino JS, et al. Diphtheria toxin-based bivalent human IL-2 fusion toxin with improved efficacy for targeting human CD25(+) cells. *J Immunol Methods*. 2014;405:57–66.
64. Becker JW, Reeke GN. Three-dimensional structure of beta 2-microglobulin. *Proc Natl Acad Sci U S A*. 1985;82(12):4225–4229.
65. Ying WZ, Aaron KJ, Sanders PW. Effect of aging and dietary salt and potassium intake on endothelial PTEN (phosphatase and tensin homolog on chromosome 10) function. *PLoS ONE*. 2012;7(11):e48715.